J Mater Sci: Mater Med (2015) 26:192
DOI 10.1007/s10856-015-5524-1

BIOCOMPATIBILITY STUDIES

Development of nanovesicular systems for dermal imiquimod delivery: physicochemical characterization and in vitro/in vivo evaluation

Man Ma[1] · Jinping Wang[1] · Fang Guo[1] · Mingzhu Lei[1] · Fengping Tan[1] · Nan Li[1]

Received: 11 November 2014 / Accepted: 8 May 2015 / Published online: 20 May 2015
© Springer Science+Business Media New York 2015

Abstract The aim of the current investigation was to develop and statistically evaluate nanovesicular systems for dermal imiquimod delivery. To this purpose, transethosomes were prepared with phospholipid, ethanol and different permeation enhancers. Conventional ethosomes, with soy phospholipid and ethanol, were used as control. The prepared vesicles were characterized for size, zeta potential, stability and entrapment efficiency. The optimal transethosomal formulation with mean particle size of 82.3 ± 9.5 nm showed the higher entrapment efficiency (68.69 ± 1.7 %). In vitro studies, permeation results of accumulated drug and local accumulation efficiency were significantly higher for transethosomes (24.64 μg/cm^2 and 6.70, respectively) than control (14.45 μg/cm^2 and 3.93, respectively). Confocal laser scanning microscopy of rhodamine 6G-loaded transethosomes revealed an enhanced retention into the deeper skin layers as compared to conventional ethosomes. Besides, Fourier-transform infra-red spectroscopy studies were also performed to understand the mechanism of interaction between skin and carriers. What's more, results of in vivo studies indicated the transethosomes of imiquimod providing the most effectiveness for dermal delivery among all of the formulations. These results suggested that transethosomes would be a promising dermal carrier for imiquimod in actinic keratose treatment.

✉ Nan Li
linan19850115@163.com

[1] Tianjin Key Laboratory of Drug Delivery & High-Efficiency, School of Pharmaceutical Science and Technology, Tianjin University, Tianjin 300072, People's Republic of China

1 Introduction

Skin cancers are by far the most common malignancies in fair skinned populations, with an incidence now reaching epidemic proportions [1, 2]. There are ~700,000 cases of cutaneous squamous cell carcinoma (cSCC) diagnosed each year in the United States and the frequency is rising worldwide [3]. An estimated 65 % of cSCC arises from precursor lesions termed actinic keratose (AK), a common skin disease characterized by cutaneous lesions due to the skin exposition to ultraviolet radiation [4]. Until now, numbers of different treatments have been tried to prevent the transformation of the cutaneous lesions into cSCC and to reduce the progression of nonmelanoma skin cancers into invasive and destructive malignant cells [5]. In this attempt, different therapeutic methods based on photodynamic therapy [6], topical therapy [7], and anticancer drugs [8, 9] are generally proposed. In particular, imiquimod (IM), administered as topical formulations, shows a certain effectiveness in the treatment of AK [10].

Imiquimod, the only immune response modifier approved for clinical applications (as Aldara®), has been successfully used to treat AK [11]. It induces, through stimulation of Toll-like receptors localized on the surface of antigen-presenting cells, the synthesis and release of several endogenous pro-inflammatory cytokines, which in turn stimulate both the innate and acquired immune pathways, resulting in upregulation of natural antiviral and antitumor activity [12]. However, highly hydrophobic nature and unsatisfactory cutaneous permeability of IM limit its therapeutic value for topical administration in form of conventional formulations (e.g., ointments).

Dermal drug delivery systems offer many advantages over other traditional routes of administration for their ability of eliminating first-pass effect, providing sustained

plasma levels and improving patient compliance. The effectiveness of dermal delivery depends on the drug's skin penetration sufficient to reach therapeutic level [13]. Unfortunately, the barrier nature of the skin presents a significant obstacle for most drugs to be delivered into and through it [14, 15]. Many delivery systems have been studied to overcome the nature barrier of stratum corneum (SC) to achieve higher dermal retention, for instance, liposomes, which have evoked considerable interest as the topical drug delivery systems [16–18].

However, it is generally agreed that the classic liposomes are of little or no value as carriers for dermal drug delivery because they can not deeply penetrate into the skin, but rather remain confined to upper layer of the SC [19]. Several researchers have reported that modification of lipid vesicular composition would lead to deformable vesicles which have superior capability to enhance dermal drug delivery. Noteworthy, ethosomal (ELs) systems, comprising of phospholipids, ethanol and water, have been proposed in the last two decades [19]. Several authors have tested different penetration enhancer molecules in the novel deformable vesicles [20, 21]. Transethosomes (TELs), which are composed of phospholipid, ethanol and permeation enhancers, have shown to possess the advantage of combining ethosomes and permeation enhancers ability to enhance the skin permeation and deposition of drug [22].

In contrast to current therapy, the therapeutic efficacy of IM in AK was related to its immune modulation. With the aim of finding nano-vesicles capable of improving IM cutaneous retention, different permeation enhancers were studied. Therefore, the current study was conducted with multiple aims: (1) to explore the superiority of nanovesicle transethosomes which performed significant skin targeting effect for dermal IM delivery; (2) to investigate the therapeutic effect, safety and mechanism of IM-loaded nano-vesicles based on in vitro and in vivo studies; and (3) to indicate the optimal transethosomes as a potential nanovehicle for IM delivery for the treatment of AK.

2 Materials and methods

2.1 Materials and animals

2.1.1 Materials

Soy phospholipid (Spc, 95 %, phosphatidylcholine) was purchased from Heowns (Tianjin, China). Imiquimod (IM, Mw 240.3, 99 % purity) was obtained from Xinghe Chemical Industry Co. (Hubei, China). Sodium dodecyl sulphate (SDS) was kindly provided by BASF SE (Ludwigshafen, Germany). Sodium deoxycholate (SDC) and oleic acid were purchased from Tianjin Guangfu Fine Chemical Research Institute (Tianjin, China). Sephadex G-50 (medium) was procured from Sigma Chemicals (St. Louis, MO, USA). Imiquimod 5 % cream (Aldara®, w/w) was obtained from 3 M Pharmaceuticals of St Paul. Trypsin and rhodamine 6G (Rh 6G) were sourced from Sigma-Aldrich (St. Louis, MO, USA). All other agents were analytical grade or better and used without further purification. Double-distilled water was used throughout the study.

2.1.2 Skin samples and animals

Skin samples were taken from the pig of about 3 months old. After removing the hair and the subcutaneous fatty tissue, the skin was cleaned in normal saline, then divided into smaller pieces and stored at −20 °C prior to use. Pharmacokinetic studies with male Sprague–Dawley rats weighing 200 ± 20 g were performed under the guidelines for humane and responsible use of animals in research set by School of Pharmaceutical Science and Technology, Tianjin University. The animals were kept in an agreeable environment with free access to a rodent diet and water and were acclimatized for at least 1 week before using.

2.2 Preparation of liposome formulations

Four different novel liposomal formulations (ELs ~ TEL3) of IM shown in Table 1 were prepared by thin film dispersion-ultrasonic method with a slight modification. Spc (final concentration of 36 mg/ml), permeation enhancers and IM (final concentration of 0.5 mg/ml) were dissolved in 25 ml chloroform–methanol (4:1, v/v). The lipid mixture was deposited as a thin film in a round-bottom flask by rotary evaporating the chloroform–methanol under reduced pressure at 35 ± 1 °C, which was applied for 1 h to ensure total removal of solvent traces. The lipid film was hydrated with 10 ml phosphate buffer solution

Table 1 Composition of various transethosomal and ethosomal formulations

Composition	Formulation code			
	ELs	TEL1	TEL2	TEL3
Spc (mg)	360	360	360	360
SDS (mg)	–	80	–	–
SDC (mg)	–	–	80	–
Oleic acid (mg)	–	–	–	40
Ethanol (ml)	2	2	2	2
PBS 5.8 (ml)	8	8	8	8
Imiquimod (mg)	5	5	5	5

(PBS, pH 5.8) containing 20 % ethanol (modifiers) by gently mixing for 1 h at room temperature and sonicated for 20 min. The sonicated vesicles were extruded through 400 nm polycarbonate membranes for further size reduction. A low pH was chosen to ensure IM encapsulation in the elastic liposome bilayer. All products were kept at 4 °C until used.

Rh 6G-labeled vesicles were prepared using an aliquot of stock solution at the concentration of 0.5 mg/ml in methanol. Briefly, Spc and 6 ml stock solution containing Rh 6G (as well as permeation enhancers if added) were added in 25 ml chloroform–methanol (4:1, v/v), then the solution was evaporated to form a lipid film on the wall of flask. The following steps were the same with the preparation of IM-loaded samples. At last, Rh 6G formulations were obtained at a final concentration of 0.03 %.

2.3 Characterization of liposomes

2.3.1 Vesicles shape

The morphology of vesicles was observed with a JEM-100 CX transmission electron microscope (TEM) (Jeol Ltd., Tokyo, Japan), with an accelerating voltage of 80 kV. A drop of diluted dispersions (1:10) was applied to a film-coated copper grid coated with carbon film and the resultant construct was then air-dried. Following this, the films were negatively stained with 0.5 % phosphotungstic acid solution and air-dried under room temperature. Then the air-dried samples were directly examined under the TEM.

2.3.2 Particle size and zeta potential measurement

The particle size and polydispersity index (PDI) for each of these vesicles were determined by the dynamic light scattering (DLS) method using a computerized particle size analyzer (Nano-ZS, Malvern, UK). The zeta potential was measured by laser-Doppler electrophoretic light scattering method using the same device. For each sample, the measurement was carried out in triplicate and the average value was recorded. Moreover, a long-term stability study was performed by monitoring the vesicle average size, PDI and zeta potential over 90 days under the environment of 4 ± 1 °C and 45 ± 10 % relative humidity.

2.3.3 Entrapment efficiency

The prepared IM-vesicles were separated from free IM using a Sephadex G-50 minicolumn (1.0 cm × 10 cm) [23]. Briefly, 0.2 ml of the IM-loaded vesicles dispersion was placed onto a Sephadex G-50 column, followed by washing for six times with 0.5 ml of PBS (pH 5.8) per time. Then the IM-vesicles nanoparticles were separated and achieved within the eluates. The eluates were vortexed for 3 min by adding methanol to break down nanovesicles. Thereafter, the amount of entrapped IM was detected using fluorescence spectroscopy (F-2700, Japan) at the emission wavelength of 340 nm, excitation wavelength of 260 nm, and slit width of 5 nm, respectively. The method was validated for selectivity, linearity, accuracy and precision. Each sample was conducted in triplicate. The EE % of IM was calculated directly from the amount of entrapped drug, according to the following equation:

$$EE\,\% = \frac{C}{T} \times 100\,\%, \tag{1}$$

where T was the initial amount of IM that was added and C was the amount of entrapped drug that was determined by a Sephadex G-50 minicolumn technique.

2.4 In vitro skin permeation studies

Permeation studies were performed according to the method described before [24] with slight modifications. Pig abdominal skin were sandwiched securely between donor and receptor compartments of the Franz Diffusion Cells (diffusion area = 1.77 cm^2, receptor volume = 17.6 ml) with the SC side facing upwards into the donor compartment. Before each experiment, the skin samples were thawed to room temperature and equilibrated at 32 ± 0.1 °C for 1 h with PBS (pH 5.8). Since pKa value of IM is 2.27, solution mixture of PBS (pH 5.8)/ethanol at 9:1 (v/v) ratio was filled in the receptor compartment for the maintenance of sink condition. The receptor compartment was continuously stirred with a small magnetic bar at a speed of 500 rpm. The IM-loaded sample (0.2 ml) was applied onto the skin surface. 2 mg of Aldara® (5 % w/w) was used as control. For each formulation, at least six replicates were carried out. Then 500 µl receptor medium was sampled at predetermined time intervals and an equal volume of receiver medium was replaced to keep a constant volume. The samples were filtered through 0.45 µm membrane filter, diluted with methanol to 2.5 ml and analyzed for drug content by fluorescence spectrophotometer as mentioned in Sect. 2.3.

At the end of the experiment (24 h), the drug retention in each skin layer was determined. The skin surface was wiped with cotton ball soaked with fresh receiver medium. SC layer was removed by tape stripping method [25]. Repeated tape-stripping (average 10 strips) was continued until SC layer was disappeared. All the strips were collected, combined, and digested in 10 ml PBS (pH 5.8). After that, the skin was cut into small sections with scissors. The tissue was further homogenized with PBS (pH 5.8)/50 % methanol (v/v) solution and then sonicated for 20 min to extract the drug. The tissue suspension were

filtered and assayed for their drug content by fluorescence spectrophotometer.

2.5 Confocal laser scanning microscopy (CLSM) study

CLSM was used to scan the fluorescence signal of fluorescence agent-loaded samples at different skin depths. During the preparation, samples were performed fluorescent by adding Rh 6G, which was similar to the properties of IM, and then applied (0.25 g) onto the skin mounted on Franz diffusion cell. After 24 h, the skin was removed and washed with distilled water. Sections of skin (20 μm thickness) were cut with a cryostat microtome perpendicular to the surface, mounted on a glass microscope slide. Analyses were carried out using a Leica TCS SP5X Inverted Supercontinuum confocal laser scanning microscope (Leica Microsystems, Heidelberg, Germany) equipped with an argon laser beam with excitation at 555 nm and emission at 560 nm. The fluorescence emission intensities and areas were analyzed by the Release Version ImageJ 1.46r analysis software (Wayne Rasband, National Institutes of Health, USA) [26]. Control images were obtained using pig skin incubated with Rh 6G-loaded ELs and tested for autofluorescence studies.

2.6 Infrared imaging spectroscopy

2.6.1 Stratum corneum isolation and sample preparation

The skin incubated with ELs, TEL1, TEL2 or TEL3 for 24 h by means of diffusion cells was the same as described in Sect. 2.4. After incubation, the skin samples were removed and residual samples on the surface of the skin was absorbed using cotton ball soaked with fresh receiver medium. The untreated skin acted as control. Then the SC was separated from the dermis by placing the skin samples on several sheets of filter paper saturated with a solution of 0.1 % trypsin in phosphate-buffered saline pH 7.4 for 5 h. The filter paper was maintained at 37 °C using thermostatic water pump. The mushy epidermis was removed from the overlying SC by digestion with trypsin for an additional 1 h. The resulting SC sheets were rinsed with cold hexane, dried at room temperature and stored in desiccator overnight. SC sheet samples were then subjected to Fourier-transform infra-red analysis. All experiments were performed in triplicate.

2.6.2 Fourier-transform infra-red spectroscopy

FTIR spectra were recorded with a Bruker TENSOR 27 spectrometer (100 scans). Spectra were acquired at a resolution of 2 cm^{-1} and the measurement range was 4000–400 cm^{-1}. All spectra were collected after baseline correction. The spectrometer was linked to a PC equipped with Bruker OPUS software to allow the automated collection of IR spectra. All measurements were performed at ambient temperature of 25 ± 1 °C. The FTIR spectrum of the control was also recorded.

2.7 In vivo skin permeation studies

Lab-made non-occlusive containers (diameter 1.5 cm), simulating Franz diffusion donor cells, were adhered on the rat dorsal skin, which had been shaved carefully to remove hair. Then infinite doses (0.3 ml of the formulations, which corresponded to 0.15 mg of IM) were topically applied into the test area. And 3 mg of Aldara® (which corresponded to 0.15 mg of IM) was used as control. At the end of the experiment, the rats were humanely sacrificed. Full thickness skin tissue were excised and rinsed in PBS (pH 5.8) to clear off the remaining formulations. The excised skin was then processed as described in the in vitro studies, and subsequently analyzed by fluorescence spectrophotometer.

2.8 Skin histological examination

Histological alteration and skin compliance after application with IM formulations were evaluated using Sprague–Dawley rats. The backside of the animals was clipped free of hair prior to the application and then 0.3 ml formulation was applied on the hair free skin with uniform spreading within the area of 1.77 cm^2. Aldara® was used as control. Autopsy samples were taken from the skin of rats in different groups and fixed in 10 % formol saline for 24 h. Paraffin bees wax tissue blocks were prepared for sectioning at 10 μm by slide microtome. The obtained tissue sections were collected on glass slides and stained by hematoxylin and eosin stains for histopathological examination through a light microscope.

2.9 Statistical analysis

Data was mean ± standard deviation (SD) from at least three independently performed experiments. The statistical analysis was assessed using a two-tailed Student's t test and a value of $P < 0.05$ was considered statistically significant.

3 Results and discussion

3.1 Vesicle formation and characterization

In the present work, nanovesicular formulations were prepared by hydrating the lipid film with different permeation

enhancers. Conventional ethosomes were also prepared for control. Four formulations were compared in terms of morphology, size, surface charge, encapsulation efficiency (Table 2) and stability.

The morphological evaluation analysis showed a small spherical or oval shape by TEM images, providing the formation of nano-vesicular (Fig. 1). Besides, it was also confirmed by the photon correlation spectroscopy that all vesicles size were between 82 and 190 nm (Table 2). It had been shown that the smaller particle size increased the penetration of encapsulated drugs into the deeper skin layers [27]. In this study, the particle size of TEL1 and TEL2 were significantly smaller ($P < 0.01$) than the control ethosomes, indicating the superior properties of the optimal formualtions. The PDI values of all nano-vesicle formulations were between 0.21 and 0.29, suggesting that all samples were sufficiently homogeneous. In general, nano-vesicles could form a stable dispersion when the absolute value of zeta potential was above 30 mv due to the electric repulsion between particles [28]. In this study, all TELs displayed a absolute negative surface charge ranging from -22.0 ± 1.1 to -29.0 ± 2.7 mv compared with -19.9 ± 2.7 mv of ELs, which might be due to the presence of permeation enhancers [29]. The relationship between net charge and size of liposomes was reported elsewhere [30], for some points of view, the more neutral net charge would result in the larger size of liposomes, which possibly due to the aggregation. Although the zeta potential values were less than 30 mv, there were no significant changes in size or zeta potential of vesicle formulations over 90 days at 4 ± 1 °C and 45 ± 10 % relative humidity (data not shown).

In addition, the EE % values of all formulations were investigated. All TEL formulations were able to incorporate a good amount of IM ranging from 68.69 ± 1.7 (TEL1) to 85.38 ± 1.4 % (TEL3) (Table 2). With the increased carbon chain length of the surfactant, the lipophilicity and the solubility of the lipophilic drug in the bilayer would be increased [31] which might explain the increase in EE % of IM in the bilayer of TELs. On the other hand, the active agents might compete with the surfactants during the process of assembling in the bilayer and therefore be excluded.

3.2 In vitro skin permeation study

The prepared formulations were subjected to in vitro release studies across pig abdominal skin. Even though new born pig skin presented a marked difference in terms of thickness, it was a good substitute for in vitro permeation study due to its similar SC with human in terms of lipid composition [32].

Cumulative amounts of permeated drug were calculated and plotted against time (Fig. 2). All formulations displayed sustained permeation of IM during the first 12 h. In the presence of surfactants (TEL1, TEL2) or oleic acid (TEL3), the permeation amount of IM was remarkably lower than that of the control group. Moreover, the percentage of maximum cumulative permeation at 24 h was only 1.37 % (for TEL3), which demonstrated that more active agents in TELs retained in the epidermis and dermis.

TEL1 formulation showed the highest Local Accumulation Efficiency [33] (LAC, 6.70) (Table 3) value followed by the TEL2 (LAC = 4.43), TEL3 (LAC = 3.58), ELs (LAC = 3.31) and commercial cream (LAC = 2.22), suggesting the obvious skin targeted effect of IM-loaded TELs compared with the control investigated formulations. The relatively higher drug deposition into the epidermis layer seemed to indicate that TELs were capable of penetrating into the hairless pig skin, reaching the target site of dermis where they formed a depot from which the drug could be released [34].

Figure 3 showed the cumulative amount of drug retained into skin layers after 24 h non-occlusive treatment. As could be seen, drug delivery was significantly enhanced by nano-vesicles in comparison with control. In the SC layer, the drug deposition significantly increased by the ELs as compared to control cream (Fig. 3). The incorporation of ethanol acted in the nano-vesicle dispersion not only affected the intercellular region of SC [35], but also softened lipid bilayers [36, 37]. As a result, more active agents were deposited into epidermal and dermal layers in the present of TELs. The improvement in the dermal delivery of active agents due to the vesicles had been related to a number of different mechanisms such as the alteration of the skin hydration [38, 39], and the increased thermodynamic activity of the drug [17]. This result also indicated

Table 2 Particle characterization of IM loaded nano-vesicles

Formulations	Vesicle size (nm ± SD)	PDI (±SD)	Zeta potential (mV ± SD)	EE (% ± SD)
ELs	190.6 ± 10	0.29 ± 0.05	−19.9 ± 2.7	41.93 ± 2.1
TEL1	82.3 ± 9.5**	0.21 ± 0.03	−29.0 ± 1.9	68.69 ± 1.7**
TEL2	92.7 ± 8.7**	0.26 ± 0.04	−28.0 ± 2.4	70.86 ± 1.2**
TEL3	142.4 ± 13*	0.28 ± 0.05	−22.0 ± 1.1	85.38 ± 1.4**

Values are the mean ± SD (n = 3) (* $P < 0.05$, ** $P < 0.01$)

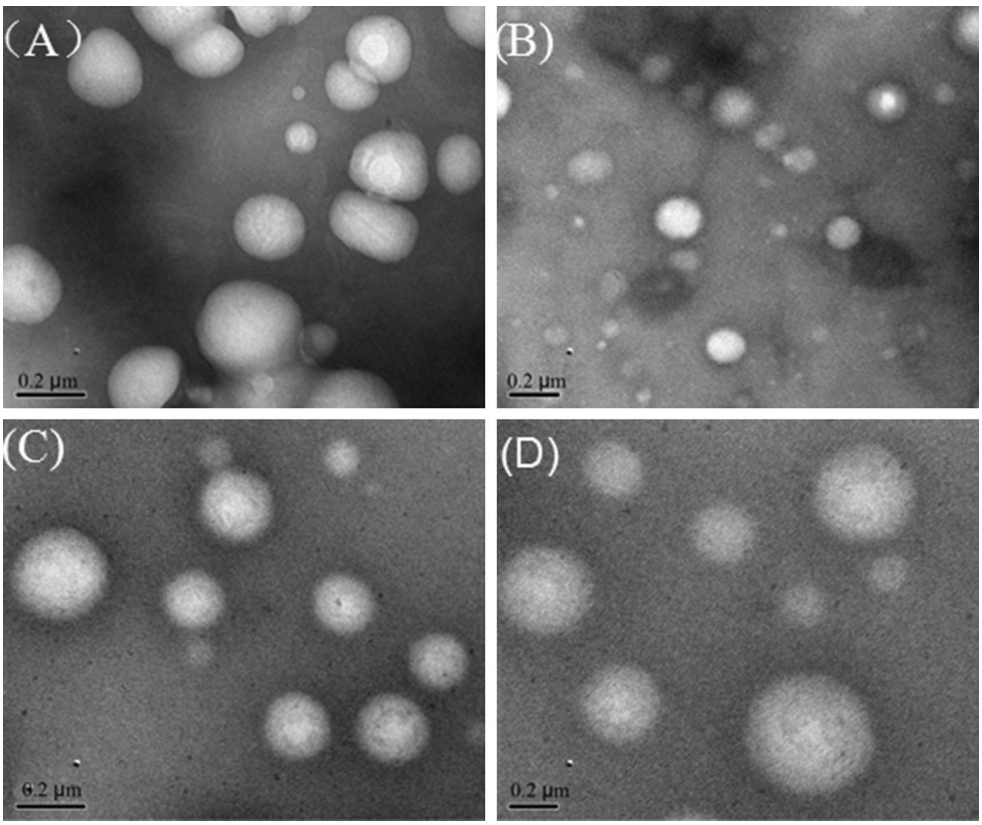

Fig. 1 TEM images of IM-loaded formulations prepared in this study. **a** Ethosomes, **b** transethosomes 1, **c** transethosomes 2, **d** transethosomes 3

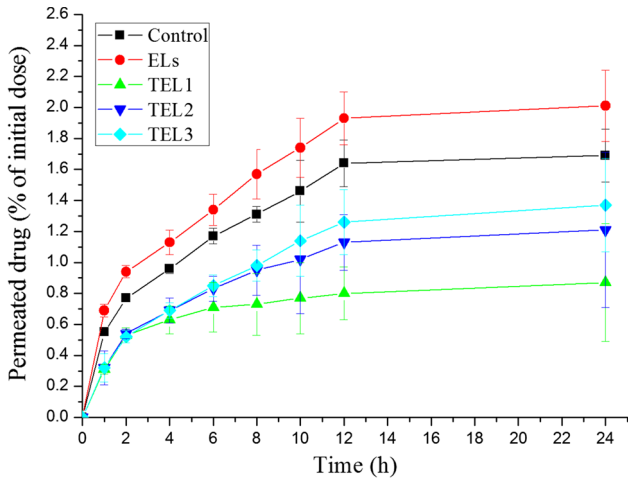

Fig. 2 In vitro diffusion of IM through pig skin from TELs in comparison with ELs and control cream. Data represent the mean ± standard deviation of at least six experimental determinations

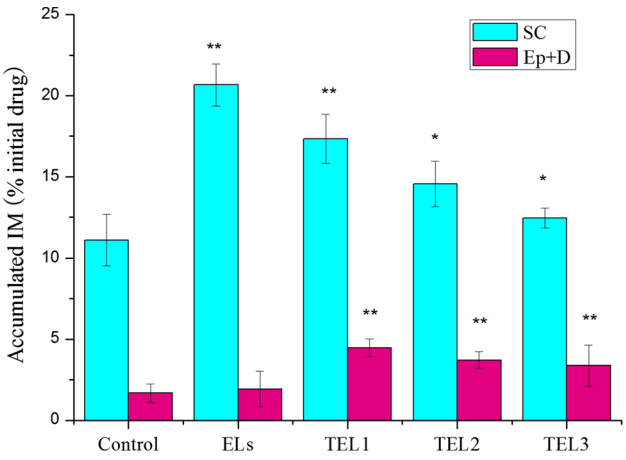

Fig. 3 Cumulative amount of IM retained into skin layers after 24 h non-occlusive treatment with vesicles suspensions and control. SC, stratum corneum; Ep, epidermis; D, dermis. Each value is the mean ± standard deviation of at least six experimental determinations ($*P < 0.05$, $**P < 0.01$)

that the TEL vesicles had the targeted effect to enhance the drug deposition in the SC and deeper skin stratum, meanwhile reduce the drug permeation into the blood for avoiding systemic side effects. In short, the in vitro permeation studies revealed superiority of the nano-vesicles compared to control.

3.3 CLSM study

CLSM study was performed to visualize the skin distribution and retention of all nanovesicles from the cross section of tissue. For these studies, a fluorescent hydrophobic label Rh

Table 3 Results of in vitro permeation study from control cream, ELs and TELs

Composition	Accumulated (μg/cm^2)	Permeated (μg/cm^2 ± SD)	LAC	J (μg/cm^2/h ± SD)
Control	14.45	6.52 ± 1.53	2.22	0.27 ± 0.03
ELs	15.53**	6.72 ± 1.61*	2.31	0.28 ± 0.07
TEL1	24.64**	3.68 ± 1.28**	6.70	0.15 ± 0.08
TEL2	20.63**	4.66 ± 1.31**	4.43	0.19 ± 0.05
TEL3	17.88**	5.00 ± 1.58*	3.58	0.21 ± 0.03

Amount of IM accumulated into the whole skin and delivered through the pig skin at the end of the experiments (24 h); LAC values; and transdermal flux (J)

Local accumulation efficiency (LAC) values: drug accumulated into the skin/drug delivered through the skin ratio. Values are the mean ± SD (n = 6) (* $P < 0.05$, ** $P < 0.01$)

6G, with an oil/water partition coefficient (Log $P = 2.69$) [40] similar to IM (Log $P = 2.27$), was added, mimic the drug, in the lipophilic phase during vesicle preparation. Figure 4 illustrated the confocal images of skin treated with Rh 6G-loaded formulations for 12 and 24 h. After 12 h, signal was found mostly in surface area, and stronger fluorescent intensity was emitted by SC layer. The fluorescence located in skin of TEL1, TEL2 and TEL3 could be seen as points with more intense red colour compared to control after 24 h. A systematic increase in fluorescence intensity suggested that the vesicular penetration was a time-dependent process. The permeation of Rh 6G via ELs was mostly restricted to the superficial epidermal layers, predominantly in the SC layer, which due to the absence of the permeation enhances for the different nano-vesicles. Therefore, compared to the control vehicle, an enhanced permeation of Rh 6G in skin layers was shown in TELs, which was consistent with in vitro penetration studies and further confirmed the targeting effect of TELs.

3.4 SC lipid organization alteration study with intact SC and FTIR

FTIR analysis provided more spectral information on the vesicles-skin interaction (Fig. 5). In the IR spectrum, the intensity of band (height and area) represented the amount of lipids/proteins in the SC. When an enhancer extracted SC lipids, these bands would show a decrease in band height and/or area or would completely disappear [41]. Hydrocarbons within the lipid domain below their transition temperature normally existed in a trans conformation. A trans gauche shift to a higher frequency (blue shift) would occur when the lipid domain became fluidized [42].

The FTIR analysis of SC provided bands at different wavenumbers, which were attributed to lipid and protein molecular vibrations in the SC [43]. In this study, untreated SC layer showed bands at 3409, 2923, 2856, 1745 and 1653 cm^{-1}. Due to the N–H and O–H stretching from lipid, protein and water, the bands were observed in range of 3000–3600 cm^{-1}. The prominent peaks obtained near 2923 and 2856 cm^{-1} respectively represented asymmetric and symmetric stretching modes of the terminal methylene groups of the lipids (ceramides, phospholipids, etc.). Meanwhile, changes in the band position from trans to gauche conformation indicated the fluidization of the lipid bilayer [44]. In addition, the small peak at 1745 cm^{-1} position was due to the lipid ester carbonyl stretch in the SC. For nano-vesicles, the bands at 1653 and 1545 cm^{-1} may represent amide 1 (C–O stretching) and amide 2 (C–N

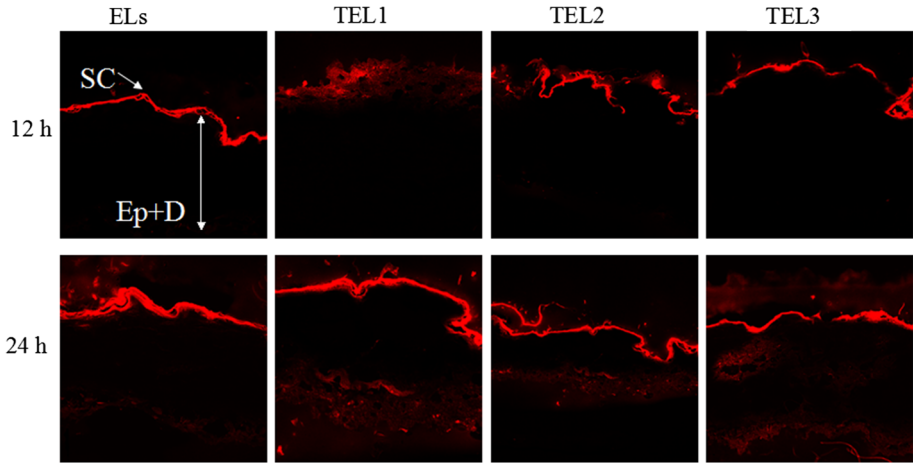

Fig. 4 CLSM micrographs of skin after in vitro application of formulations for 12 and 24 h. Images showed the distribution of fluorescence into the stratum corneum (SC), epidermis and dermis (Ep + D). Image size: 1024 × 1024 pixels, where each pixel = 0.625 μm for ×40 objective

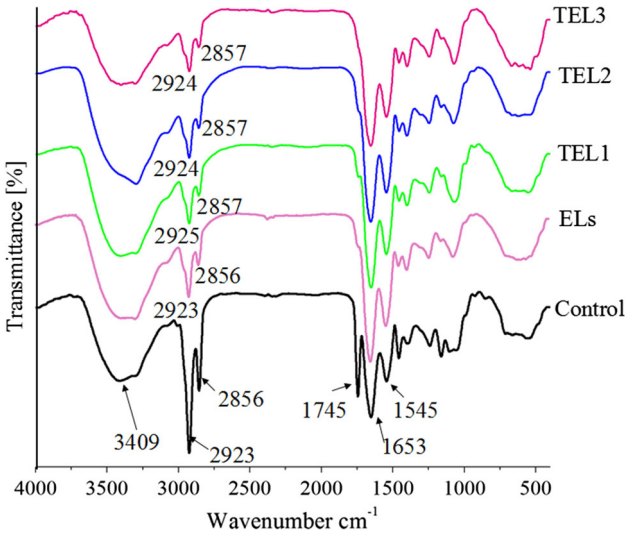

Fig. 5 The FTIR spectra of untreated SC and SC treated with prepared vesicles

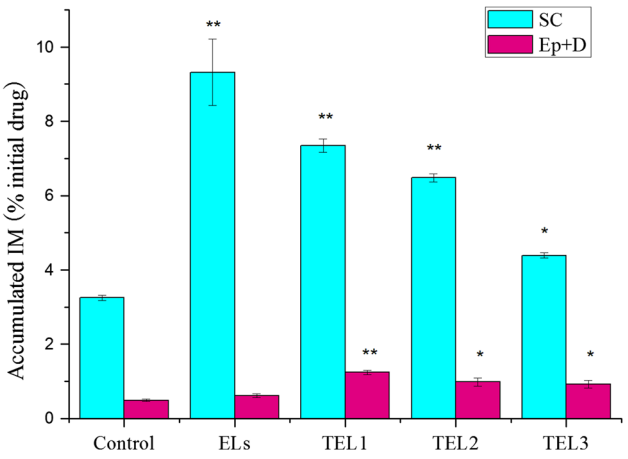

Fig. 6 Cumulative amount of drug accumulated into the skin layers after in vivo treatment with vesicular suspensions and control cream. SC, stratum corneum; Ep, epidermis; D, dermis. Each value is the mean ± standard deviation of at least six experimental determinations (*$P < 0.05$, **$P < 0.01$)

stretching) linkages of the helical secondary structure found in epidermal keratin [45].

Blue shifts at 2925 and 2857 cm^{-1} which shown in the spectral analysis of TELs (Fig. 5) indicated lipid bilayer fluidization and SC hydration. These shifts and the 1735 cm^{-1} band were also accompanied with a decrease in peak heights, suggesting that lipid extraction was generated. After treatment with ethosomal samples, reduced peak intensity at 2923 and 1745 cm^{-1} may be related to extraction of lipid which due to presence of alcohols in the formulations. In general, FTIR data indicated that TELs formulations enhanced permeation of active agents mainly by fluidization and extraction of lipid bilayer.

3.5 In vivo skin deposition study

In vivo skin deposition experiments were conducted to further study the distribution of drug in different skin layers (SC, epidermal and dermal) after administration with nano-vesicles and control Aldara® (Fig. 6). After 24 h, the amount of drug deposited in the SC and epidermis/dermis of Sprague–Dawley rat skin was measured by fluorescence spectrophotometer. As shown in Fig. 6, the in vivo skin deposition showed the same tendency as the in vitro skin results, however, the IM retention in skin layers in vivo was lower than that in vitro, which might be due to the thinner skin of rat compared with pig. Moreover, the improved skin permeability of TELs might be related to the nano-vesicle deformability and the smaller particle-size distribution. As a result, in the epidermis/dermis, the in vivo skin deposition in conjunction with TELs was significantly higher than that of Aldara®. Thus, the modified IM-loaded nano-vesicles had the potential to deliver the effective amount of drugs to the targeted site in skin layers. In addition, novel nano-vesicles could enable the maintenance of their localized depot and, therefore, prolong residence time for the treatment of AK.

Blood samples were also collected in these preparation groups, unfortunately, IM concentration in the blood during 24 h was below the limit of determination, which indicated the lower side effect in in vivo studies.

3.6 Histological examinations

To evaluate the biocompatibility of IM-loaded nano-vesicles on dorsal skin of mice, we investigated histopathological features of treated skin. Nano-vesicles and cream were assessed in the same way.

Histopathological images (Fig. 7) showed neither significant thickening of the skin layers, nor an accumulation of inflammatory cell nucleus in the inflamed skin layer. The rat epidermis remained intact with no obvious changes and stratified squamous cells arranged closely comprised epithelial tissue. As compared with control, no inflammatory reaction was observed in skin which exposed to the test formulations, indicating that the nano-vesicles were biocompatibility. The results demonstrated that using phospholipids alone or in conjunction with ethanol or permeation enhances lead to hardly any irritation of the skin for short time application.

4 Discussion

The greatest obstacle for dermal delivery is the barrier property of the SC. Many approaches have been used to breach the skin barrier; for example, the use of lipid nano-

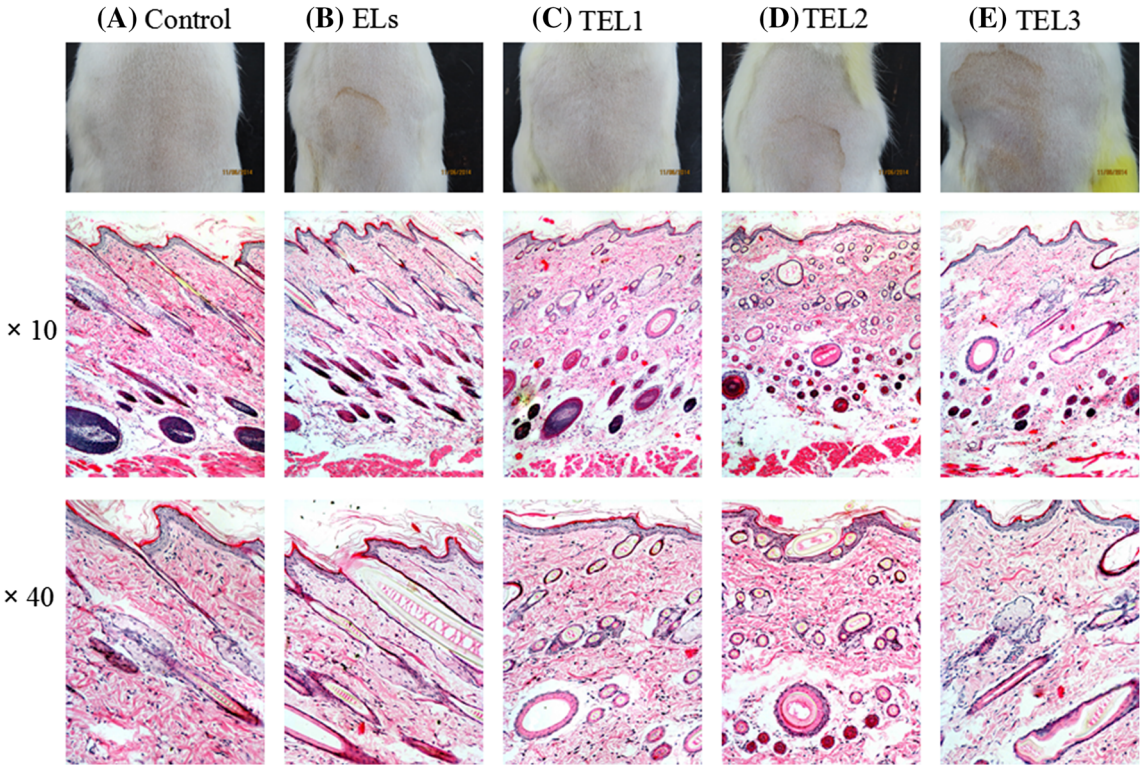

Fig. 7 Wistar rats skin appearance after treatment and representative images of skin tissues after H&E staining

vesicles to modulate the SC is gaining interest. Furthermore, the incorporation of ethanol in lipid nano-vesicles (ELs) is a good approach to fluidize the skin lipid membrane and accordingly enhance drug deposition and provision. The ethanol can interact with the polar head group region of the lipid molecules, resulting in the reduction of the melting point of the SC lipid, thereby increasing lipid fluidity and cell membrane permeability [46].

However, the use solely of ethanol in preparation of ELs often leads to excessive transdermal drug flux, and therefore, unsatisfactory skin deposition [47]. Previous reports have revealed that ethanol combined with penetration enhancer in vesicles can significantly enhance the skin deposition of drugs [48].

It has been reported that the H-bonding capability of a penetration enhancer is one of the major factors in determining its skin penetration behavior [49, 50]. The most powerful H-bonding lipid in the SC layer is ceramide 6, which had four secondary alcohol and one secondary amide groups [51]. Thus, interactions among ceramide 6 molecules are believed to represent the major intermolecular binding among SC lipids [52].

Penetration enhancers, such as SDS, SDC, and oleic acid, could intercalate into skin lipids due to its long lipophilic hydrocarbon chain, loosen up intermolecular binding among SC lipids, and increase the skin permeability. On the other hand, sulfo group (for SDS, SDC) and carboxyl group (for oleic acid) have an extra oxygen atom which could form additional H-bonding with adjacent ceramide head groups, raising the possibility of crosslinking to both. Therefore the selected penetration enhancers could positively affect the physico-chemical properties of phospholipid vesicles and synergically improve the dermal delivery of loaded IM.

5 Conclusion

In the present study, TELs, combining the advantages of penetration enhancers and modifiers, were prepared and characterized, and their efficacy as potential carriers for skin IM delivery was also evaluated. CLSM and in vitro/vivo skin permeation/deposition testing suggested superior aptness of IM-loaded TELs to ELs, which might be due to greater solubility, retentivity, and adaptability in lipid bilayers consisting of permeation enhancers. FTIR data indicated that TELs formulations enhanced permeation of active agents mainly by fluidization and extraction of lipid bilayer. Histological examinations further confirmed the biocompatibility of nano-carriers by showing no inflammatory cell infiltration or erythema in dorsal skin. These findings demonstrated that topical administration of IM-

loaded TELs might become a promising target treatment for local AK.

Acknowledgments The National Basic Research Project (2014CB 932200) of the MOST acknowledged for financial support.

References

1. Madan V, Lear JT, Szeimies RM. Non-melanoma skin cancer. Lancet. 2010;375(9715):673–85.
2. Rogers HW, Weinstock MA, Harris AR, Hinckley MR, Feldman SR, Fleischer AB, Coldiron BM. Incidence estimate of non-melanoma skin cancer in the United States. Arch Dermatol. 2006;146(3):283–7.
3. De Vries E, De Poll-Franse V, Louwman WJ, et al. Predictions of skin cancer incidence in the Netherlands up to 2015. Br J Dermatol. 2005;152(3):481–8.
4. Criscione VD, Weinstock MA, Naylor MF, Luque C, Eide MJ, Bingham SF. Actinic keratoses: natural history and risk of malignant transformation in the Veterans Affairs Topical Tretinoin Chemoprevention Trial. Cancer. 2009;115(11):2523–30.
5. Cohen JL. Actinic keratosis treatment as a key component of preventive strategies for nonmelanoma skin cancer. J Clin Aesthet Dermatol. 2010;3:39–44.
6. Stritt A, Merk HF, Braathen LR, von Felbert V. Photodynamic therapy in the treatment of actinic keratosis. Photochem Photobiol. 2008;84:388–98.
7. Weinberg JM. Topical therapy for actinic keratoses: current and evolving therapies. Rev Recent Clin Trials. 2006;1:53–60.
8. Li L, Shukla S, Lee A, Garfield SH, Maloney DJ, Ambudkar SV, Yuspa SH. The skin cancer chemotherapeutic agent ingenol-3-angelate (PEP005) is a substrate for the epidermal multidrug transporter (ABCB1) and targets tumor vasculature. Cancer Res. 2010;70:4509–19.
9. Resnick L, Rabinovitz H, Binninger D, Marchetti M, Weissbach H. Topical sulindac combined with hydrogen peroxide in the treatment of actinic keratoses. J Drugs Dermatol. 2009;8:29–32.
10. Hadley G, Derry S, Moore RA. Imiquimod for actinic keratosis: systematic review and meta-analysis. J Invest Dermatol. 2006;126:1251–5.
11. Swanson N, Abramovits W, Berman B, Kulp J, Rigel DS, Levy S. Imiquimod 2.5 % and 3.75 % for the treatment of actinic keratoses: results of two placebo-controlled studies of daily application to the face and balding scalp for two 2-week cycles. J Am Acad Dermatol. 2010;62:582–90.
12. Lacarrubba F, Nasca MR, Micali G. Advances in the use of topical imiquimod to treat dermatologic disorders. Ther Clin Risk Manag. 2008;4:87–97.
13. Dos Anjos JL, Alonso A. Terpenes increase the portioning and molecular dynamics of an amphipathic spin label in stratum corneum membranes. Int J Pharm. 2008;350:103–12.
14. Aqil M, Ahad A, Sultana Y, Ali A. Status of terpenes as skin penetration enhancers. Drug Discov Today. 2007;12:1061–7.
15. Ahad A, Aqil M, Kohli K, Chaudhary H, Sultana Y, Mujeeb M, Talegaonkar S. Chemical penetration enhancers: a patent review. Exp Opin Ther Pat. 2009;19:969–88.
16. Chourasia MK, Kang L, Chan SY. Nanosized ethosomes bearing ketoprofen for improved transdermal delivery. Results Pharm Sci. 2011;1:60–7.
17. Mahale NB, Thakkar PD, Mali RG, Walunj DR, Chaudhari SR. Niosomes: novel sustained release nonionic stable vesicular systems—an overview. Adv Colloid Interface Sci. 2012;183–184:46–54.
18. Sinico C, Fadda AM. Vesicular carriers for dermal drug delivery. Expert Opin Drug Deliv. 2009;6:813–25.
19. Touitou E, Dayan N, Bergelson L, Godin B, Eliaz M. Ethosomes-novel vesicular carriers for enhanced delivery: characterization and skin penetration properties. J Control Release. 2000;65:403–18.
20. Dragicevic-Curic N, Scheglmann D, Albrecht V, Fahr A. Temoporfin-loaded invasomes: development, characterization and in vitro skin penetration studies. J Control Release. 2008;127:59–69.
21. Manconi M, Mura S, Sinico C, Fadda AM, Vila AO, Molina F. Development and characterization of liposomes containing glycols as carriers for diclofenac. Colloids Surf A. 2009;342:53–8.
22. Song CK, Balakrishnan P, Shim CK, et al. A novel vesicular carrier, transethosome, for enhanced skin delivery of voriconazole: characterization and in vitro/in vivo evaluation. Colloids Surf B Biointerfaces. 2012;92:299–304.
23. Duangjit S, Opanasopit P, Rojanarata T, Ngawhirunpat T. Characterization and in vitro skin permeation of meloxicam-loaded liposomes versus transfersomes. J Drug Deliv. 2010;2011.
24. Caon T, Costa AC, de Oliveira MA, Micke GA, Simoes CM. Evaluation of the transdermal permeation of different paraben combinations through a pig ear skin model. Int J Pharm. 2010;391:1–6.
25. Jain S, Tiwary AK, Sapra B, Jain NK. Formulation and evaluation of ethosomes for transdermal delivery of lamivudine. AAPS Pharm Sci Tech. 2007;8:111.
26. Wang JP, Guo F, Ma M. Development of ketoconazole nanovesicular system using 1,2-hexanediol and 1,4-cyclohexanediol for dermal targeting delivery: physicochemical characterization and in vitro/in vivo evaluation. J Nanopart Res. 2014;16:2505.
27. Verma DD, Verma S, Blume G, Fahr A. Particle size of liposomes influences dermal delivery of substances into skin. Int J Pharm. 2003;258:141–51.
28. Chen Y, Wu QQ, Zhang ZH, Yuan L, Liu X, Zhou L. Preparation of curcumin-loaded liposomes and evaluation of their skin permeation and pharmacodynamics. Molecules. 2012;17:5972–87.
29. Balakrishnan P, Shanmugam S, Lee WS, et al. Formulation and in vitro assessment of minoxidil niosomes for enhanced skin delivery. Int J Pharm. 2009;377:1–8.
30. Roy M, Gallardo M, Estelrich J. Influence of size on electrokinetics behavior of phosphatidylserine and phosphatidylethanolamine lipids vesicles. J Colloid Interface Sci. 1998;206:512–7.
31. Mohammed AR, Weston N, Coombes AGA, Fitzgerald M, Perrie Y. Liposome: formulation of poorly water soluble drugs: optimisation of drug loading and ESEM analysis of stability. Int J Pharm. 2004;285(1–2):23–34.
32. Cilurzo F, Minghetti P, Sinico C. New born pig skin as model membrane in in vitro drug permeation studies: a technical note. AAPS Pharm Sci Technol. 2007;8:E1–4.
33. Manconi M, Caddeo C, Sinico C, et al. Ex vivo skin delivery of diclofenac by transcutol containing liposomes and suggested mechanism of vesicle–skin interaction. Eur J Pharm Biopharm. 2011;78(1):27–35.
34. Honeywell-Nguyen PL, Groenink HW, Bouwstra JA. Elastic vesicles as a tool for dermal and transdermal delivery. J Liposome Res. 2006;16:273–80.
35. Touitou E, Godin B, Weiss C. Enhanced delivery of drugs into and across the skin by ethosomal carriers. Drug Dev Res. 2000;50:406–15.
36. Paolino D, Lucania G, Mardente D, Alhaique F, Fresta M. Ethosomes for skin delivery of ammonium glycyrrhizinate: in vitro percutaneous permeation through human skin and in vivo anti-inflammatory activity on human volunteers. J Control Release. 2005;106:99–110.

37. Godin B, Touitou E. Erythromycin ethosomal systems: physico-chemical characterization and enhanced antibacterial activity. Curr Drug Deliv. 2005;2:269–75.
38. Müller RH, Radtke M, Wissing SA. Solid lipid nanoparticles (SLN) and nanostructured lipid carriers (NLC) in cosmetic and dermatological preparations. Adv Drug Deliv Rev. 2002;54: S131–55.
39. Esposito E, Drechsler M, Mariani P, et al. Nanosystems for skin hydration: a comparative study. Int J Cosmetic Sci. 2007;29(1):39–47.
40. Lampidis TJ, Castello C, Del Giglio A, Pressman BC, Viallet P, Trevrrow KW, Valet GK, Tapiero H, Savaraj N. Relevance of the chemical charge of rhodamine dyes to multiple drug resistance. Biochem Pharmacol. 1898;38:4267–71.
41. Laugel C, Yagoubi N, Baillet A. ATR-FTIR spectroscopy: a chemometric approach for studying the lipid organisation of the stratum corneum. Chem Phys Lipids. 2005;135:55–68.
42. Ibrahim SA, Li SK. Chemical enhancer solubility in human stratum corneum lipids and enhancer mechanism of action on stratum corneum lipid domain. Int J Pharm. 2010;383:89–98.
43. Garidel P. Mid-FTIR-Microspectroscopy of stratum corneum single cells and stratum corneum tissue. Phys Chem Chem Phys. 2002;4(22):5671–7.
44. Panchagnula R, Salve PS, Thomas NS, Jain AK, Ramarao P. Transdermal delivery of naloxone: effect of water, propylene glycol, ethanol and their binary combinations on permeation through rat skin. Int J Pharm. 2001;219(1–2):95–105.
45. Mendelsohn R, Chen HC, Rerek ME, Moore DJ. Infrared microspectroscopic imaging maps the spatial distribution of exogenous molecules in skin. J Biomed Opt. 2003;8(2):185–90.
46. Elsayed MA, Abdallah YO, Naggar FV, Khalafallah NM. Lipid vesicles for skin delivery of drugs: reviewing three decades of research. Int J Pharm. 2006;332:1–16.
47. Zhang JP, Wei YH, Zhou Y, Li YQ, Wu XA. Ethosomes, binary ethosomes and transfersomes of terbinafine hydrochloride: a comparative study. Arch Pharm Res. 2012;35:109–17.
48. Guo F, Wang JP, Ma M, Tan FP, Li N. Skin targeted lipid vesicles as novel nano-carrier of ketoconazole: characterization, in vitro and in vivo evaluation. J Mater Sci. 2015;26:175.
49. Abraham MH, Chdha HS, Mitchell RC. The factors that influence skin penetration of solutes. J Pharm Pharmacol. 1995;47:8–16.
50. Roberts MS, Pugh WJ, Hadgraft J. Epidermal permeability-penetrant structure relationships: 2. The effect of H-bonding groups in penetrants on their diffusion through the stratum corneum. Int J Pharm. 1996;132:23–32.
51. Wertz PW. Epidermal lipids. Semin Dermatol. 1992;11:106–13.
52. Hadgraft J, Peck J, Williams DG, Pugh WJ, Allan G. Mechanisms of action of skin penetration enhancers/retarders: azone and analogues. Int J Pharm. 1996;141:17–25.